ELSEVIER

Colloids and Surfaces
A: Physicochemical and Engineering Aspects 182 (2001) 109–122

COLLOIDS AND SURFACES A

www.elsevier.nl/locate/colsurfa

An energy balance approach to modeling the hydrodynamically driven spreading of a liquid drop

David Erickson, Byron Blackmore, Dongqing Li *

Department of Mechanical and Industrial Engineering, University of Toronto, Toronto, Ontario, Canada M5S 3G8

Received 12 April 2000; accepted 11 December 2000

Abstract

This paper extends the overall energy balance (OEB) approach to the modeling of liquid drop spreading to cases where the primary motive force is hydrodynamic in nature. In such cases the mass, and therefore total energy, of the system varies with time thus invalidating previous OEB models. By relating the change in internal energy of the drop with the energy entering the system, changes in potential energy and work done by the system, a non-linear first-order ordinary differential equation has been developed which describes the drop spreading process for the case of a spherical cap of constant dynamic contact angle and constant mass flow rate. To provide validation data for the model, an experimental study has also been undertaken. In these experiments the Axisymmetric Drop Shape Analysis technique has been used to monitor the changing contact angle and contact radius of the drop as it advances across a solid surface. The solution of the ODE is shown to be in very good agreement with the experimental results, until such time as the drop grows to beyond the range where the spherical cap approximation is valid. A comparison of the magnitude of the energetic terms has revealed that the major deterrent to drop spreading is the work required to increase the surface area of the drop. In the case of slow speed spreading, it is shown that the viscous dissipation at the three-phase line is negligible, leading to a model completely free of any empirically determined curve fitting factors.

Keywords: Liquid drop spreading; Moving contact line; Overall energy balance

1. Introduction

The spreading of a viscous liquid drop on a solid surface is a problem of both fundamental concern and practical interest. Applications range from large scale industrial lubrication to ink-jet printing, from spray cooling to road wetting, and adhesion to metal forming in material processing. A large number of reviews have been written on the subject of drop spreading and wettability and are available elsewhere [1–4].

Generally, previous papers have addresses the study of drop spreading in one of two-ways, as a classical fluid mechanics problem [5–7] or through a surface physics approach [8–10]. Two major difficulties arise from the fluid mechanics approach: modeling the slip condition at the

* Corresponding author.
E-mail address: dli@mie.utoronto.ca (D. Li).

0927-7757/01/$ - see front matter
PII: S0927-7757(00)00834-7

three-phase line and determining the relationship between the dynamic contact angle and the velocity of the advancing contact radius [6]. The surface physics approach has revealed that the spreading process is dependent largely on the interfacial tensions and contact angles as well as various chemical, physical and quantum mechanical parameters, which may or may not be possible to determine [11]. Models resulting from the combination of the two approaches have been successful, however they are generally largely dependent on empiricism to quantify the solution [11].

Other researchers [12–16] have studied the relationship between dynamic contact angle and the advancing speed of the three-phase line. A number of these studies have developed simple, semi-empirical equations, which generally relate the dynamic contact angle to the capillary number plus a 'shift factor' [12]. For example Kalliadasis and Chang [16] use a precursor film model and scaling arguments to develop the relationship $\tan\theta_d = [\tan^3\theta_e - 9\log\ \eta Ca]^{1/3}$, where Ca is the capillary number, η is a scaled Hamaker constant, and θ_e and θ_d are the equilibrium and dynamic contact angles.

In principal a general theoretical model for drop spreading must account for not only the motion of the bulk phase but also the continuous changes in the surface and line phases, viscous dissipation, gravitational potential energy and wettability. Mathematically this kind of motion over a solid surface is described by high order differential equations to even the crudest of approximations.

Madejski [17] is likely the first to employ an overall energy balance (OEB) approach to model drop spreading, specifically considering the solidification of impinging drops on a cold surface. In that paper Madejski proposed that the change in the total surface and kinetic energy of the drop must be completely balanced by the internal viscous dissipation, thus yielding Eq. (1) (using the nomenclature of this paper):

$$\frac{d}{dt}(E_k + E_s + W_v) = 0, \tag{1}$$

where E_k, E_s and W_v are the internal kinetic energy, surface potential energy and work of viscous dissipation, respectively. Madejski determined the internal kinetic energy by assuming a simple velocity profile within the drop and then used this profile to estimate the internal viscous dissipation using Newton's law. Surface energy was calculated by considering only the change in area of the liquid–vapour interface. San Marchi et al. [18] used Madejski's manipulation of the energy components in Eq. (1) as a basis for their model of impinging drops with partial solidification.

More recently Gu and Li have used the OEB approach to model both spontaneous [19] and low speed impact [20] drop spreading. Their analysis yielded a similar OEB equation to that of Madejski's (for completeness the gravitational potential energy was also considered, but found to be negligible), however their calculation of the energy components was dramatically different. In their approach a numerical simulation of the impacting drop was used to determine the internal velocity profile and thus the internal kinetic energy. Dissipation work was calculated by considering the viscous force at the three-phase line. A more exact approach to the surface energy term was taken by considering the changes in the surface areas of all three interfaces (liquid–vapor, liquid–solid and solid–vapor). Their model proved very successful in modeling spontaneous spreading, and was found to slightly overestimate the growth rate for higher speed impacting.

Generally, dynamic wetting can be classified into two broad categories [15], spontaneous and forced, the latter of which can be further classified by the primary motive force. Spontaneous spreading can be thought of as the migration of liquid drop over a solid surface as it approaches thermodynamic equilibrium. It is this type of spreading that the original model by and Gu and Li [19] was originally designed to simulate.

The more general and industrially applicable case is that of forced spreading. In the case of the Madejski [17] and second Gu and Li paper [20] the primary driving force was the initial kinetic energy of a drop of fixed mass. In many applications the primary driving force is hydrodynamic in nature, meaning that drop spreading is accomplished through the addition of liquid (mass) to

the system. This is the essential mechanism in some industrial coating processes, polymer processing technologies (such as mold filling) and welding. A common method of failure in these cases is the inability of the fluid to displace sufficient surface area quick enough, thus limiting the speed at which the process can be done [15]. As a result simple and reliable models of predicting the drop spreading speed are required.

In this paper we will extend the OEB model of drop spreading to account for the more general case of hydrodynamically-driven drop spreading. As will be shown the overall energy balance is dramatically different for this case than those previous examples, due to the addition of mass, and therefore energy, to the system. Since the geometry of the drop spreading process can vary dramatically from application to application, a general derivation using a spherical cap approximation will be presented. By using a similar evaluation of the applicable energy terms as the Gu and Li model, we will show how this drop spreading phenomena can be modeled using a numerical solution to an ordinary differential equation with little or no degree of empiricism. A comparison of the magnitudes of the various energetic terms will be conducted and their effect on the overall drop spreading process will be discussed. An experimental study has also been undertaken to provide validation data for the OEB model. The experiments use the Axisymmetric Drop Shape Analysis [21] technique to measure the changes in contact radius and dynamic contact angle as the drop advances across the surface.

2. Formulation of the OEB drop spreading model

Fig. 1 shows a schematic of a growing non-volatile droplet on a smooth, rigid and homogeneous solid surface. The primary driving force behind drop spreading in this case is the quasi-steady addition of liquid to the system through a hole in the surface (at point O). In the following analysis it has been assumed that the drop spreads axisymmetrically about this point and that it is in thermal equilibrium with its surroundings. In general the dynamic contact angle, θ_d, the contact radius, R, and the advancing speed of the three phase line (or drop spreading speed), dR/dt, all vary as a function of time.

As mentioned Section 1, previous energy balance approaches to drop spreading have considered only the case of a drop of fixed mass impinging on a solid surface. There are many engineering applications where the addition of energy to the system (in the form of mass transfer) is the primary motive force behind spreading, thus invalidating these previous models. A more general OEB equation would consider the amount of energy transferred to the system and the total internal energy of the system in addition to the applicable potential energy and work terms, which are the basis of the previous energy balance models. Thus for the case shown in Fig. 1, the energy entering the system (E_{in}) is balanced with the change in internal energy of the system (E_{sys}), increase or decrease in surface (E_s) and gravitational (E_g) potential energies, boundary movement work (W_b), and the viscous dissipation work (W_v). Thus the OEB equation for the system shown in Fig. 1 is given by Eq. (2):

$$\frac{dE_{in}}{dt} = \frac{d}{dt}(E_{sys} + E_s + E_g) + \frac{d}{dt}(W_v + W_b). \qquad (2)$$

In general Eq. (2) may contain a heat transfer term on the right hand side to account for any heat transferred from or to the drop during the spreading process. However, for the case of a liquid drop in thermal equilibrium with its surroundings and negligible internal heat generation, such as the case here and in previous OEB models [17,19,20], this term can be ignored. Each of the terms in Eq. (2) will be examined separately in the following sections.

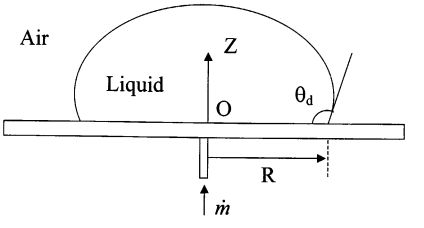

Fig. 1. Schematic diagram of the hydrodynamically forced spreading of a sessile drop on a solid surface.

2.1. Energy transferred to the system, E_{in}

For the case of interest in this study, the energy transferred to the system for an arbitrary change in mass Δm is defined by the enthalpy and kinetic energy of the liquid entering the system at O, as shown in Eq. (3) [22]:

$$\Delta E_{\text{in}} = \Delta m \left[h(T_o) + \frac{v^2}{2} \right], \tag{3}$$

where $h(T_o)$ is the enthalpy evaluated at the systems equilibrium temperature T_o and v is the entrance velocity. Redefining the enthalpy term according to its definition yields:

$$\Delta E_{\text{in}} = \Delta m \left[u(T_o) + \frac{P}{\rho} + \frac{v^2}{2} \right], \tag{4}$$

where P is the absolute pressure of the fluid at the jet entrance, ρ is its density and $u(T_o)$ its internal energy. In general both u and h are functions of both pressure and temperature however for incompressible liquids, such as those examined here, the dependence on pressure is negligible.

In principal an exact value for the entrance pressure can be determined through a numerical solution to the Laplace equation of capillarity. For small drop sizes however (such as those considered here) or small differences between the densities of the drop and its surrounding medium, surface forces will dominate and the droplet will assume a basically spherical shape. In such a case the pressure difference will be uniform throughout the drop and equal to the sum of the Laplace and atmospheric pressures, as given by Eq. (5):

$$P = \frac{2\gamma_{\text{lv}} \sin(\theta_{\text{d}})}{R} + P_o \tag{5}$$

where γ_{lv} is surface tension of the liquid–vapor interface. By combining Eq. (4) and Eq. (5) and considering an infinitesimal change in mass with respect to time, Eq. (6) is obtained which is the sought after rate of change of incoming energy as a function of time:

$$\frac{\mathrm{d}E_{\text{in}}}{\mathrm{d}t} = \left[u(T_o) + \frac{1}{\rho} \left(\frac{2\gamma_{\text{lv}} \sin(\theta_{\text{d}})}{R} + P_o \right) + \frac{v^2}{2} \right] \frac{\mathrm{d}m}{\mathrm{d}t}. \tag{6}$$

2.2. Internal energy of the system, E_{sys}

Analogous to the previous section the total internal energy of the system is defined as the sum of the internal energy and kinetic energy terms. In principal the total internal kinetic energy of the drop should be evaluated by integrating the velocity profile over its volume, as is done in previous OEB models. By an order of magnitude analysis (in Appendix A), it is shown that the internal kinetic energy of the drop can be ignored when the surface area of the sessile drop is significantly larger than the area of the liquid jet. As this is the case for most examples of hydrodynamically driven drop spreading, the internal kinetic energy will be ignored and only the internal energy u will be considered. Although the temperature of the system remains constant, the total internal energy changes with the amount of mass in the system as per Eq. (7):

$$\Delta E_{\text{sys}} = [(m + \Delta m)\, u(T_o) - m u(T_o)]. \tag{7}$$

Reducing the above equation and considering an infinitesimal change in mass with respect to time yields Eq. (8):

$$\frac{\mathrm{d}E_{\text{sys}}}{\mathrm{d}t} = u(T_o) \frac{\mathrm{d}m}{\mathrm{d}t}. \tag{8}$$

2.3. Surface potential energy, E_s

The total surface energy of the system is equivalent to the sum of the grand canonical free energy of the three interfacial phases (liquid–solid, liquid–vapor and solid–vapor):

$$E_{\text{s}} = \gamma_{\text{ls}} A_{\text{ls}} + \gamma_{\text{sv}} A_{\text{sv}} + \gamma_{\text{lv}} A_{\text{lv}}, \tag{9}$$

where γ and A represent the surface tension and area of the three interfacial phases described above. Differentiating with respect to time and recognizing the equality between the change in solid–vapor and solid–liquid surface areas yields the change in surface potential energy with time, Eq. (10):

$$\frac{\mathrm{d}E_{\text{s}}}{\mathrm{d}t} = (\gamma_{\text{sl}} - \gamma_{\text{sv}}) \frac{\mathrm{d}A_{\text{sl}}}{\mathrm{d}t} + \gamma_{\text{lv}} \frac{\mathrm{d}A_{\text{lv}}}{\mathrm{d}t}. \tag{10}$$

For a homogeneous, rigid and smooth solid surface the surface tensions can be related using Young's equation:

$$\gamma_{lv} \cos \theta_e = \gamma_{sv} - \gamma_{sl}, \tag{11}$$

where θ_e is the equilibrium contact angle which is in general not equivalent to the dynamic contact angle. The change in the solid–liquid and liquid–vapor surface areas of an axisymmetric and spherical drop can be estimated from Eqs. (12a) and (12b) and Eq. (12c):

$$\frac{dA_{sl}}{dt} = 2\pi R \frac{dR}{dt}, \tag{12a}$$

$$\frac{dA_{lv}}{dt} = 4\pi R h(\theta_d) \frac{dR}{dt} + 2\pi R^2 \frac{dh(\theta_d)}{dt}, \tag{12b}$$

$$h(\theta_d) = \frac{1 - \cos \theta_d}{\sin^2 \theta_d}. \tag{12c}$$

Combining Eqs. (10), (11) and 12 results in the total change in the surface potential energy, given by Eq. (13) below:

$$\frac{dE_s}{dt} = 2\pi R \gamma_{lv} [2h(\theta_d) - \cos \theta_e] \frac{dR}{dt} + 2\pi R^2 \gamma_{lv} \frac{dh(\theta_d)}{dt}. \tag{13}$$

2.4. Gravitational potential energy, E_g

The change in the gravitational potential energy for an arbitrary change of mass, Δm, is dependent on two variables, the total mass in the system and the change in the height of the center of gravity, Δz, as described by Eq. (14):

$$\Delta E_g = g [(m + \Delta m)(z + \Delta z) - mz], \tag{14}$$

where g is the acceleration due to gravity and z is the location of the center of mass. In evaluating this term it is important to realize that buoyancy effects have been neglected. In the case where the density difference between the drop and its surrounding medium is small, the buoyancy effect on this term would have to be considered. Expanding Eq. (14), eliminating the higher order terms and again considering an infinitesimal change with respect to time yields the general gravitational potential energy term, Eq. (15):

$$\frac{dE_g}{dt} = g \left[m \frac{dz}{dt} + z \frac{dm}{dt} \right]. \tag{15}$$

To evaluate this term, assuming dm/dt is known, requires knowledge of the total mass of the system and location of its center of gravity. The former of these can be determined through evaluation of Eq. (16):

$$m = m_o + \int_0^t \frac{dm}{dt} dt, \tag{16}$$

where m_o is the initial mass of the system, which can be estimated from the initial radius, R_o, and contact angle as below:

$$m_o = \frac{\pi \rho R_o^3 (1 - \cos \theta_d)^2 (2 + \cos \theta_d)}{3 \sin^3 \theta_d}. \tag{17}$$

For a spherical drop it can be shown that the center of mass is given by Eq. (18a) Eq. (18b):

$$z = \frac{R}{4} f(\theta_d), \tag{18a}$$

$$f(\theta_d) = \frac{6 \sin^2 \theta_d - 3(1 - \cos \theta_d)^2 - 8(1 - \cos \theta_d)\cos \theta_d}{(2 + \cos \theta_d)\sin \theta_d}. \tag{18b}$$

Thus the general result for the change in the center of gravity with respect to time is given by Eq. (19):

$$\frac{dz}{dt} = \frac{f(\theta_d)}{4} \frac{dR}{dt} + \frac{R}{4} \frac{df(\theta_d)}{dt}. \tag{19}$$

Combining Eqs. (15), (18) and (19) yields the desired relation for the change in gravitational potential energy with respect to time:

$$\frac{dE_g}{dt} = g \left[m \left(\frac{f(\theta_d)}{4} \frac{dR}{dt} + \frac{R}{4} \frac{df(\theta_d)}{dt} \right) + \frac{R}{4} f(\theta_d) \frac{dm}{dt} \right]. \tag{20}$$

2.5. Boundary movement work, W_b

In the case of the fixed mass, or more appropriately fixed volume, droplets considered in the previous OEB treatments obviously the boundary movement work must be identically zero. In the present treatment however, work must be done to displace the atmospheric pressure as the drop grows beyond its original volume. For an arbitrary change in volume, ΔV, against a constant

atmospheric pressure, this is expressed by the well know equation shown below:

$$\Delta W_b = P_o \Delta V. \tag{21}$$

Again we consider an infinitesimal change in volume with respect to time to obtain the desired result, Eq. (22):

$$\frac{\mathrm{d}W_b}{\mathrm{d}t} = \frac{P_o}{\rho}\frac{\mathrm{d}m}{\mathrm{d}t}. \tag{22}$$

2.6. Viscous dissipation work, W_v

The de Gennes framework for dissipative losses has recently been employed successfully to model wetting behavior in a number of cases [19,20,23]. In his work [24] de Gennes concluded that for low-speed spreading the hydrodynamic losses dominate over molecular forces and derived the following formula for the viscous force per unit length of three-phase line:

$$F_v(t) = \frac{3\mu}{\theta_\mathrm{d}} \ln(\varepsilon^{-1}) \frac{\mathrm{d}R}{\mathrm{d}t}, \tag{23}$$

where μ is the liquid viscosity and $\varepsilon_\delta = L_\delta/L$ is the ratio of the microscopic to macroscopic cut-off lengths. L_δ is the cut-off length below which the continuum theory breaks down and is though to vary from 1 to 5 μm. L is proportional to the horizontal length scale of the liquid drop, thus $L = R$. Detailed information on the application of this ratio to drop spreading is available elsewhere [19]. By multiplying Eq. (23) with the velocity of the advancing front ($\mathrm{d}R/\mathrm{d}t$) and integrating over the three-phase line, the viscous dissipation work per unit time is obtained as below:

$$\frac{\mathrm{d}W_\mathrm{v}}{\mathrm{d}t} = 6\pi\mu \ln(\varepsilon^{-1})\frac{R}{\theta_\mathrm{d}}\left(\frac{\mathrm{d}R}{\mathrm{d}t}\right)^2. \tag{24}$$

2.7. General OEB equation

Combining the results of Sections 2.1, 2.2, 2.3, 2.4, 2.5 and 2.6 with the general OEB Eq. (2) yields the following general differential equation describing the spreading of a viscous drop on a homogeneous, smooth, solid surface:

$$\left[6\pi\mu \ln(\varepsilon^{-1})\frac{R}{\theta_\mathrm{d}}\right]\left(\frac{\mathrm{d}R}{\mathrm{d}t}\right)^2 + \left[2\pi R\gamma_\mathrm{lv}[2h(\theta_\mathrm{d}) - \cos\theta_\mathrm{e}] + mg\frac{f(\theta_\mathrm{d})}{4}\right]\frac{\mathrm{d}R}{\mathrm{d}t} + \frac{\mathrm{d}m}{\mathrm{d}t}\left[\frac{gR}{4}f(\theta_\mathrm{d}) - \frac{2\gamma_\mathrm{lv}\sin(\theta_\mathrm{d})}{\rho R} - \frac{v^2}{2}\right] + 2\pi R^2\gamma_\mathrm{lv}\frac{\mathrm{d}h(\theta_\mathrm{d})}{\mathrm{d}t} + mg\frac{R}{4}\frac{\mathrm{d}f(\theta_\mathrm{d})}{\mathrm{d}t} = 0, \tag{25a}$$

where $f(\theta_\mathrm{d})$ and $h(\theta_\mathrm{d})$ are as defined above. In principal Eq. (25a) relates the speed of the advancing contact radius to the material properties and the dynamic contact angle. It should be noted that the effect of the solid surface on which the drop is spreading, is accounted for in the above model by the solid–vapor and solid–liquid free energies, related to the equilibrium contact angle through Young's Eq. (11). Since the total mass of the drop, m as calculated from Eq. (16), appears in the above equation, Eq. (25a) is in general a non-linear, ordinary, integro-differential equation which must be solved numerically. By subjecting it to an appropriate initial condition, i.e. $R(t = 0) = R_o$, the above equation can be solved using a Runge–Kutta technique for the contact radius as a function of time, assuming that the dynamic contact angle and its time derivatives are either known or can be estimated from one of the relations/techniques described elsewhere [12–16]. Additionally a description of $\mathrm{d}m/\mathrm{d}t$ must be available, such that at each time step, m can be recalculated using Eq. (16). It is also important to note that in Eq. (25a) the only curve-fitting term is the ratio of macroscopic to microscopic cut-off lengths, ε.

In the case of a constant dynamic contact angle and constant mass flow rate, $\mathrm{d}m/\mathrm{d}t = \dot{m}$, Eq. (25a) can be simplified to the form shown below:

$$\left[6\pi\mu \ln(\varepsilon^{-1})\frac{R}{\theta_\mathrm{d}}\right]\left(\frac{\mathrm{d}R}{\mathrm{d}t}\right)^2 + \left[2\pi R\gamma_\mathrm{lv}[2h(\theta_\mathrm{d}) - \cos\theta_\mathrm{e}] + (m_o + \dot{m}t)g\frac{f(\theta_\mathrm{d})}{4}\right]\frac{\mathrm{d}R}{\mathrm{d}t} + \dot{m}\left[\frac{gR}{4}f(\theta_\mathrm{d}) - \frac{2\gamma_\mathrm{lv}\sin(\theta_\mathrm{d})}{\rho R} - \frac{v^2}{2}\right] = 0. \tag{25b}$$

Table 1
Comparison of energy balance methods

Energetic terms	Madejski [17]	Gu and Li [19,20]	Current model
Energy transferred to the system (dE_{in}/dt)	N/A	N/A	Enthalpy and kinetic energy of entering fluid
Internal kinetic and internal energy of the system (dE_{sys}/dt)	Assumed internal velocity profile to determine kinetic energy	Numerical calculation of internal velocity to determine kinetic energy	Change of total internal energy due to the addition of mass dominating over internal kinetic energy
Surface potential Energy (dE_s/dt)	Change in *l–v* interfacial area	Change in *l–v*, *l–s*, *s–v* interfacial areas	Change in *l–v*, *l–s*, *s–v* interfacial areas
Gravitational Potential Energy (dE_s/dt)	Not considered	Mass center approach (found to be negligible)	Mass center approach
Boundary movement work (dW_b/dt)	N/A	N/A	Work done to displace the environmental pressure
Viscous dissipation work (dW_v/dt)	Assumed internal velocity profile, Newton's Law	de Gennes framework for dissipation at three phase line	de Gennes framework for dissipation at three phase line

It is this form of Eq. (25a) that will be used to validate the OEB method in Section 3 by modeling the hydrodynamically driven spreading of an oil droplet over a solid surface.

2.8. Summary of OEB approaches

To emphasize the considerable differences between this and previous OEB approaches to drop spreading, Table 1 presents a comparison of this method with the two previous models outlined in Section 1. As mentioned the previous methods only consider the spreading of a drop of fixed mass, whereas here a hydrodynamically driven system of variable mass is considered.

3. Experimental study of drop spreading

In order to validate the above model several experiments were conducted using MCT-30 oil (Imperial Oil product) advancing on a glass slide coated with FC-725 (a fluorocarbon coating, 3M product). The experimental fluid has the following physical properties; viscosity $\mu = 0.286$ N s m^{-2}, density $\rho = 879.2$ kg m^{-3}, surface tension $\gamma_{lv} = 31.16$ mJ m^{-2} and equilibrium contact angle = 78.6°. Five tests were conducted at two different mass flow rates, 2.76 and 3.11 mg min^{-1}.

A schematic of the experimental set-up is shown in Fig. 2. As mentioned above the spreading surface was a glass slide coated with FC-725 to ensure that roughness and surface inhomogeneity effects would be negligible. A 250 μm diameter hole was drilled in the center of the plate, which was supported on an anti-vibration table and insured to be level prior to beginning all tests. One end of a 200 μm (outside diameter) capillary tube was inserted and fixed into the hole while the other end was fitted with a flexible nylon tubing which connected to the syringe pump. The motorized syringe was driven by an Anaheim Automation Miniangle stepper motor (Model #

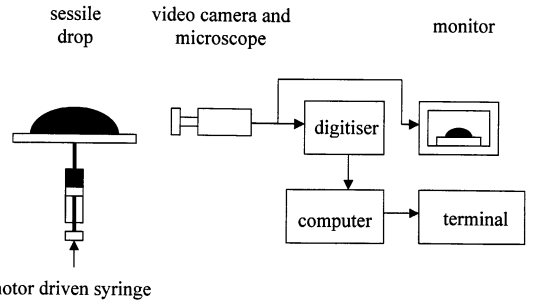

Fig. 2. Experimental set-up for dynamic contact angle and contact radius measurements using the Axisymmetric Drop Shape Analysis technique.

23PM-C402) and controlled by an Anaheim Automation (Model # DPF72) Controller.

The critical aspect of this experiment is the ability to accurately measure the changes in contact radius and dynamic contact angle as the drop advances across the surface. The automated Axisymmetric Drop Shape Analysis (ADSA) technique [21] combined with a digital image analysis and processing system is a powerful tool for making such measurements. In previous studies, this technique has been applied to the study of many capillary phenomena including the drop size dependence of contact angles and surface tension ageing [21].

The ADSA computer image system is depicted in Fig. 2. A Cohu 4910 CCD monochrome camera is mounted upon a Leica wild M3B microscope. The video signal generated is transmitted first to a Sanyo B/W Video Monitor and then to a VideoPix digital video processor. The video processor was used to record the signal and digitize the image to a resolution of 640×480 pixels with 256 gray levels. A Sun Sparc 10 Unix computer was used to operate the digital video processor and to analyze the data. The Axisymmetric Drop Shape Analysis software package was utilized to acquire the drop images at different times, digitize the recorded images and to determine the drop's contact diameter and the advancing contact angle as a function of time.

To conduct a test the syringe plunger was first advanced at a slow rate until a drop of suitable size was visible on the surface. After allowing the drop to settle to equilibrium, the syringe was set to advance (at a constant speed) once again and the image analysis system began recording and saving an image every 10 s, which was later processed using the ADSA technique outlined above. In each run a nearly constant dynamic contact angle was observed as shown in Table 2. The error associated with assuming a constant θ_d was $\pm 1°$ over the course of any single run. All experiments were conducted at room temperature, 22°C.

This process was repeated several times and for two different syringe plunger speeds (corresponding to the high and low mass flow rates mentioned earlier). At each trial, a freshly prepared glass slide was used to ensure that the surface was not prewetted with the experimental fluid.

Table 2
Measured dynamic contact angles

Mass flow rate (mg min^{-1})	Run	Dynamic contact angle (°)
2.76	#1	81 ± 1
	#2	82 ± 1
	#3	79 ± 1
3.11	#1	79 ± 1
	#2	80 ± 1

4. Results and discussion

Fig. 3(a and b) show the measured values of the contact radius, using the ADSA technique described in Section 3, as the drop advanced across the surface for the five runs at the two separate mass flow rates (2.76 and 3.11 mg min^{-1}). A range of initial contact radii has been selected in order to test the model over a variety of initial conditions. In each case the drop was allowed to reach a stable dynamic contact angle first.

4.1. Comparison of OEB relation with experimental results

Using the starting contact radii shown in Fig. 3(a and b) as an initial condition and the dynamic contact angles shown in Table 2, the OEB relation, Eq. (25b), was solved using a forth order Runge–Kutta technique. The results are shown as solid lines superimposed over the raw data. The initial mass of the drop was estimated by the spherical cap approximation outlined in Section 2.5 and the ratio of the microscopic to macroscopic cut-off lengths, ε, was taken as a constant value of 0.005 in accordance with the value used by Gu and Li [19].

As can be seen in the two figures the solution to the OEB equation models the experimental data well over the range of tested values until such time as the drop becomes so large such that the spherical cap approximation is no longer representative

of the true drop shape. In each case once the drop grows beyond a certain limit, the model tends to predict a slower advancing velocity than is actually observed.

As mentioned in Section 2.1 the model calculates the pressure at point O (see Fig. 1) by assuming a spherical shape and therefore constant pressure field within the drop, defined by Eq. (5). Since this value varies with $1/R$ and the hydrostatic pressure varies approximately with R, as the drop grows the Laplace pressure will become less significant and the hydrostatic, which the model ignores, more significant. As a result the value of dE_{in}/dt in Eq. (6) is likely to be underestimated at these larger drop sizes resulting in the slower than observed advancing velocity shown at the tail end

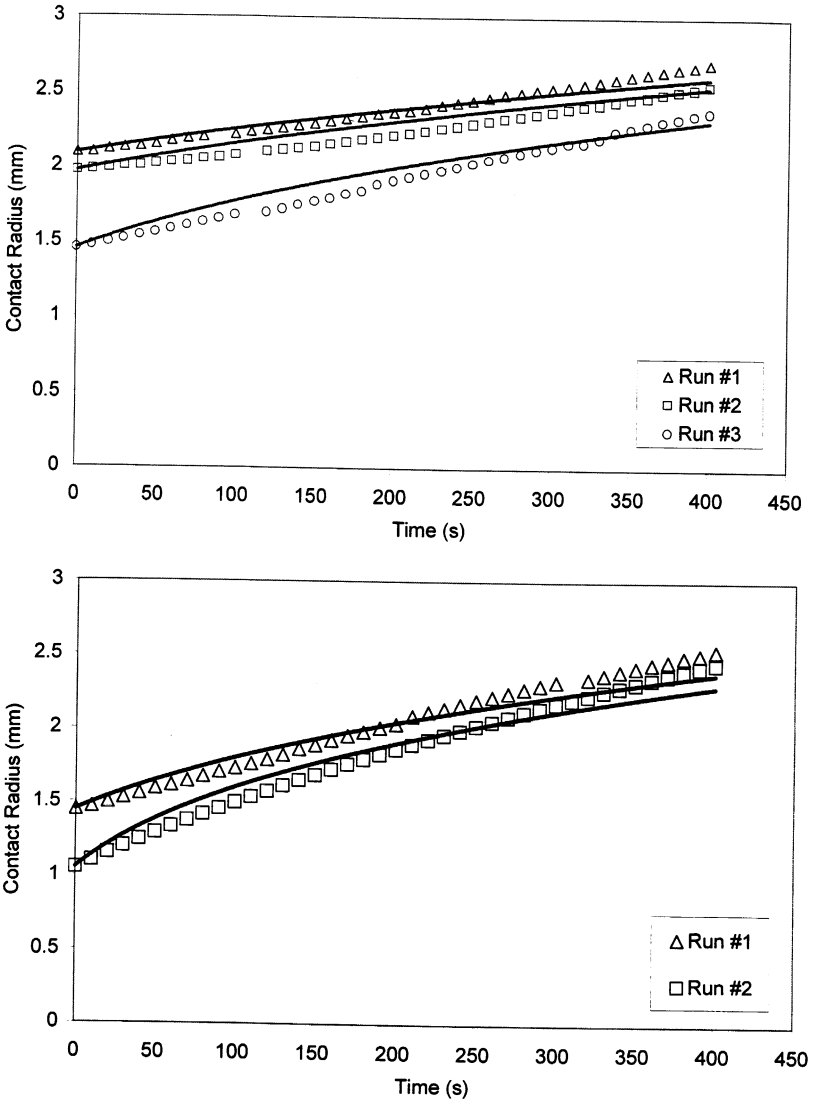

Fig. 3. (a) Comparison of measured contact radius and model prediction for slow spreading (mass flow rate = 2.76 mg min^{-1}) of MCT-30 oil on FC-725 surface. Solid lines represent model prediction and hollow symbols represent experimental data; (b) Comparison of measured contact radius and model prediction for the fast spreading (mass flow rate = 3.11 mg min^{-1}) of MCT-30 oil on FC-725 surface. Solid lines represent model prediction and hollow symbols represent experimental data.

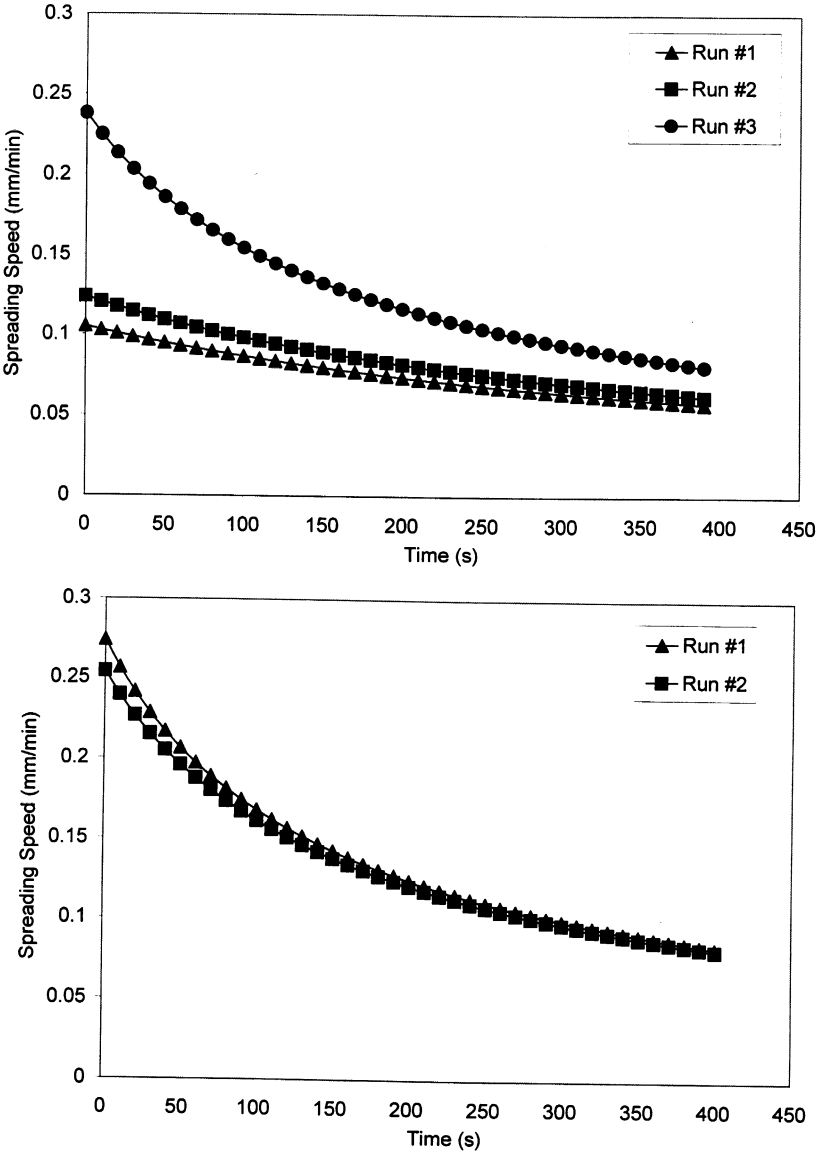

Fig. 4. (a) Predicted speed of advancing contact radius (dR/dt) for the slow spreading case (mass flow rate = 2.76 mg min^{-1}); (b) Predicted speed of advancing contact radius (dR/dt) for the fast spreading case (mass flow rate = 3.11 mg min^{-1}).

of the results. Additionally as the drop grows and the surface forces become less significant, the drop will begin to flatten out and the spherical assumption will likely overestimate the work done in a gravitational field and underestimate the surface area growth. In order to model larger drop sizes a more complex and accurate model of the true drop shape [19,20] would have to be used.

4.2. Drop spreading velocity

Of interest in most of the engineering applications, mentioned earlier, is the speed at which the drop spreads over the surface. Fig. 4(a and b) show the energy model prediction of the drop spreading speed for the two different mass flow rates. Intuitively it would be expected that the

advancing front would slow down as the drop size grows since mass is being added to the system at a constant rate. This is trend is indeed reflected by the OEB model, as shown in Fig. 4(a and b), and is well established in the Fig. 3(b) for high mass flow rate case. In the low mass flow rate case it is likely that the total amount by which the drop grows is to small to notice this trend.

Knowledge of the drop spreading velocity is critical in the determining the applicability of the lubrication theory approximation, used in the derivation of the viscous force formula at the three-phase line, to this situation. Batchelor [25] gives the following constraint where such an approximation is valid:

$$\theta_d \frac{\rho R}{\mu} \frac{dR}{dt} \ll 1. \quad (26)$$

In this study the value of this parameter is generally of the order 10^{-3}, thus validating the applicability of this model in predicting the viscous dissipation at the three-phase line.

4.3. Comparison of energetic components

Critical to the modeling of any phenomena through thermodynamic methods is a firm understanding of the relative magnitude of each of the energetic terms being considered. Gu and Li [19] showed a comparison of the relative importance of the applicable terms for the case of spontaneous spreading. Their results showed that for all practical purposes the viscous dissipation work was completely balanced by the reduction in the total surface energy and that the change in gravitational potential energy was negligible.

Fig. 5 shows an analogous plot of energetic consumption by or contribution to the system by the terms outlined in Section 2 for a representative run. Terms on the right hand side of Eq. (2) can be though of as prohibitive to drop spreading and are thus given a negative magnitude. For ease of comparison with the remaining terms, the energy entering the system, E_{in}, change in total internal energy, E_{sys}, and boundary movement work, W_b, have been com-

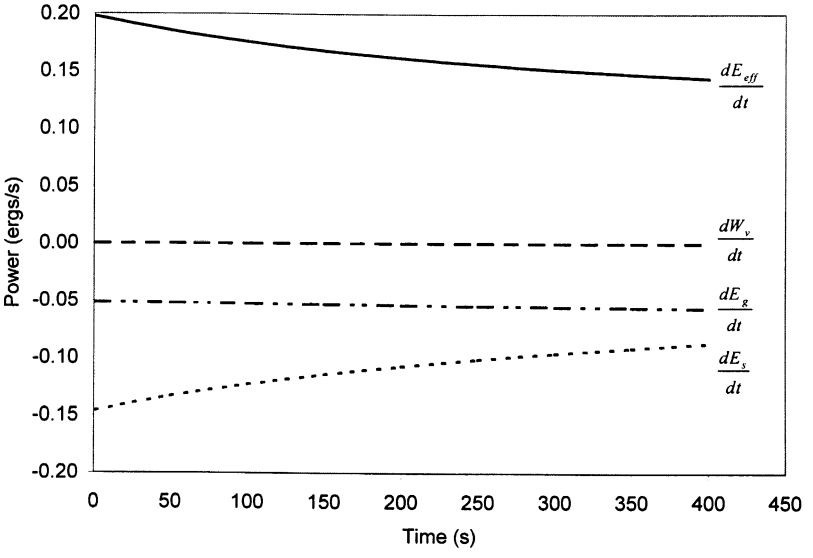

Fig. 5. Comparison of the energy consumption and delivery by the effective energy and work terms for hydrodynamically driven drop spreading. Run #2 of the fast spreading case (mass flow rate = 3.11 mg min^{-1}) is presented as a representative example.

bined and can be though of as the effective amount of usable energy delivered to the system, E_{eff}.

In this case the effective energy delivered to the system is nearly completely balanced by the work done in increasing the total surface energy and the work done against gravity. Over the range of tested values the gravitational term varies from 35 to 65% of the magnitude of the surface energy term. The general downward trend in the effective energy delivered to the system is caused by the decrease in the Laplace pressure, and thus Eq. (6), as the drop grows. Physically this can be interpreted as a decrease in the total flow work done in pumping the liquid into the system. The surface and gravitational potential terms each show opposite trends with the magnitude of the former decreasing and the latter increasing slightly as the drop grows. Of course as the total mass of the drop increases the work required to raise it in a gravitational field should also. The decreasing trend in the magnitude of the surface energy consumption is the result of the slowing of the advancing contact radius velocity, observed in Section 4.2.

The negligible effect of the viscous dissipation at the three-phase line, shown in Fig. 5, is a consequence of the slow speed of the advancing contact radius. As can be seen in Eq. (25b) it varies with the square of dR/dt while all other terms are linear, thus the relative importance of this term will decrease with the decreasing spreading velocity. A consequence of this is that when the spreading velocity is slow enough, such as the case examined here, the viscous term can be omitted from Eq. (25b), leaving a completely general model for drop spreading which contains no curve fitting factors.

When Fig. 5 is compared with the results for spontaneous or surface tension dominated spreading mentioned earlier, there are several differences of note. Most immediately is the fact that for the hydrodynamically-driven drop spreading, the work required to change its surface areas is the largest energy consumer. In the case of spontaneous spreading, this change in surface area, to lower to total free energy of the system, is the main driving force behind drop spreading. The other significant difference is the relative magnitude of the gravitational potential energy term. In Eq. (20) it is shown that dE_g/dt is dependent on both the total mass of the drop and the mass flow rate (dm/dt). Obviously for the fixed mass case dm/dt would be zero, thus this term would be omitted all together. Additionally the drops consider here are much more massive than those considered by Gu and Li increasing the relative importance of the first term.

5. Conclusions

The study of the drop spreading on a flat solid surface is an excellent example of the interplay between a classical fluid mechanics and a surface physics problem. In general previous models of this phenomena have involved complex numerical solutions which may or may not be physically intuitive or been highly dependent on empiricism to quantify the model. In this paper an overall energy balance (OEB) approach was undertaken to model the spreading of a hydrodynamically-driven drop of variable mass and energy over a solid surface. The model balances the amount of energy delivered to the system with the change in internal energy, changes in surface and gravitational potential energy, and boundary movement and viscous dissipation work. The resulting first order ODE was solved for the case of a spherical cap using a simple Runge–Kutta technique and the results compared with those obtained from an experimental study.

In general it was shown that the OEB solution did successfully model the spreading phenomenon very well until such time as the drop grew beyond the range where the spherical cap approximation was valid. As intuitively expected the model predicted a decrease in the velocity of the advancing front as the drop grew in volume. A comparison of the energetic magnitude of the various terms was conducted and it was shown that in this case the effective energy delivered to the system is balanced by the increase in total surface energy and gravitational potential energy, with the former having approximately twice the magnitude of the latter. Additionally it was shown that when

the drop spreading is slow enough the viscous dissipation at the three-phase line is negligible and the OEB approach yielded a model completely free of any empirically determined curve fitting factors. Thus in such a case the drop spreading phenomena can be entirely modeled with knowledge of the material properties and an estimation of the dynamic contact angle. The method itself is not explicitly constrained to small droplets, however a more flexible final solution would have to involve a numerical computation of the true drop shape at each step.

Acknowledgements

The authors wish to thank the financial support of the Natural Sciences and Engineering Research Fund through scholarships to David Erickson and Byron Blackmore, and through a research grant to D. Li.

Appendix A. Order of magnitude analysis for kinetic energy terms

As a method of simplifying the analysis it was proposed in Section 2.2 that the change in the internal kinetic energy of the drop was negligible compared with the kinetic energy of the fluid entering the system, and thus it could be effectively ignored. By an order of magnitude analysis the conditions under which this assumption is valid will be investigated.

From Eq. (6) the kinetic energy transferred to the system ($E_{\mathrm{in},k}$) over an infinitesimal change in time is given by:

$$\frac{\mathrm{d}E_{\mathrm{in},k}}{\mathrm{d}t} = \frac{v^2}{2}\frac{\mathrm{d}m}{\mathrm{d}t}, \tag{A1}$$

where v is the velocity of the liquid entering the drop. Recognizing that v is of the order of $\dot{m}/\rho A_{\mathrm{in}}$, where A_{in} is the area of the entrance, and substituting $\dot{m}$ for $\mathrm{d}m/\mathrm{d}t$ yields the following expression for the order of magnitude of $\mathrm{d}E_{\mathrm{in},k}/\mathrm{d}t$:

$$\frac{\mathrm{d}E_{\mathrm{in},k}}{\mathrm{d}t} = O\left[\frac{\dot{m}^3}{2\rho^2}\frac{1}{A_{\mathrm{in}}^2}\right]. \tag{A2}$$

The change in the internal kinetic energy of the drop due to the addition of mass is given by Eq. (A3):

$$\Delta E_{\mathrm{sys},k} = \int_0^{V+\Delta V} \rho\frac{v^2}{2}\,\mathrm{d}V - \int_0^{V} \rho\frac{v^2}{2}\,\mathrm{d}V, \tag{A3}$$

where v is the internal velocity of the fluid and V is the volume of the drop. If fluid is being added at a constant rate, by continuity the velocity profile over a given region in a spherically growing drop must remain constant, thus Eq. (A3) reduces to:

$$\Delta E_{\mathrm{sys},k} = \int_{V}^{V+\Delta V} \rho\frac{v^2}{2}\,\mathrm{d}V. \tag{A4}$$

Recognizing that v in the region formed by the addition of mass is of the order $\dot{m}/\rho A_{\mathrm{lv}}$, where A_{lv} is the area of the liquid–vapor interface, Eq. (A5) is obtained:

$$\Delta E_{\mathrm{sys},k} = O\left[\frac{\rho}{2}\left(\frac{\dot{m}}{\rho A_{\mathrm{lv}}}\right)^2 \Delta V\right]. \tag{A5}$$

Reducing the above to an infinitesimal change with respect to time and recognizing that $\mathrm{d}V/\mathrm{d}t = \dot{m}/\rho$, yields the following estimate for the order of magnitude of $\mathrm{d}E_{\mathrm{sys,k}}/\mathrm{d}t$:

$$\frac{\mathrm{d}E_{\mathrm{sys},k}}{\mathrm{d}t} = O\left[\frac{\dot{m}^3}{2\rho^2}\frac{1}{A_{\mathrm{lv}}^2}\right]. \tag{A6}$$

Comparing the two results, as is done in Eq. (A7), suggests that when the surface area of the drop is much greater than the area through which the fluid enters, the kinetic energy of the fluid entering the drop will dominate. For the case of a spherically growing drop on a flat surface where initial drop radius is larger than the entrance radius, such as that considered here, this condition is always met thus it is justifiable to ignore the internal kinetic energy of the system.

$$\frac{\mathrm{d}E_{\mathrm{in},k}/\mathrm{d}t}{\mathrm{d}E_{\mathrm{sys},k}/\mathrm{d}t} = O\left[\left(\frac{A_{\mathrm{lv}}}{A_{\mathrm{in}}}\right)^2\right]. \tag{A7}$$

References

[1] E.B. Dussan, Ann. Rev. Fluid Mech. 11 (1979) 371.
[2] A. Marmur, Adv. Colloid Interface Sci. 19 (1983) 75.

[3] P.G. de Gennes, Rev. Mod. Phys. 57 (1985) 827.
[4] J.C. Berg, Wettability, Marcel Dekker, New York, 1993.
[5] H.P. Greenspan, J. Fluid Mech. 84 (1978) 125.
[6] P.J. Haley, M.J. Miksis, J. Fluid Mech. 223 (1991) 57.
[7] D.M. Koch, D.L. Koch, J. Fluid Mech. 287 (1995) 251.
[8] B.W. Cherry, C.M. Holmes, J. Colloid Interface Sci. 29 (1969) 174.
[9] T.D. Blake, J.M. Haynes, J. Colloid Interface Sci. 30 (1969) 421.
[10] M.D. Lelah, A. Marmur, J. Colloid Interface Sci. 82 (1981) 518.
[11] F.T. Dodge, J. Colloid Interface Sci. 121 (1988) 154.
[12] R.L. Hoffman, J. Colloid Interface Sci. 50 (1975) 228.
[13] R.E. Johnson, R.H. Dettre, D.A. Brandreth, J. Colloid Interface Sci. 62 (1977) 205.
[14] J.-D. Chen, J. Colloid Interface Sci. 122 (1988) 60.
[15] T.D. Blake, in: J.C. Berg (Ed.), Wettability, Marcel Dekker, New York, 1993 Chapter 5.
[16] S. Kalliadasis, H.-C. Chang, Ind. Eng. Chem. Res. 35 (1996) 2860.
[17] J. Madejski, Int. J. Heat Mass Trans. 19 (1976) 1009.
[18] C. San Marchi, H. Liu, E.J. Lavernia, R.H. Rangel, A. Sickinger, E. Muehlberger, J. Material Sci. 28 (1993) 3313.
[19] Y. Gu, D. Li, Colloids Suf. A 142 (1998) 243.
[20] Y. Gu, D. Li, Colloids Suf. A 163 (2000) 239.
[21] D. Li, P. Cheng, A.W. Neumann, Adv. Colloid Interface Sci. 39 (1992) 347.
[22] G. Van Wylen, R. Sonntag, C. Borgnakke, Fundamentals of Classical Thermodynamics, 4th, John Wiley and Sons, 1993.
[23] S. Basu, K. Nandakumar, J.H. Masliyah, J. Colloid Interface Sci. 182 (1996) 82.
[24] F. Brochard-Wyart, P.G. de Gennes, Adv. Colloid Interface Sci. 39 (1992) 1.
[25] G.K. Batchelor, An Introduction to Fluid Dynamics, Cambridge University Press, Cambridge, 1967, p. 220.